Chapter 5
Experimental Determination of Thermal Expansion Using Digital Image Correlation and Thermoresistive Sensing in MWCNT-Integrated Polymer-Bonded Energetics

Viswajit Talluru, Arend Austria, Pranay Anekal, and Gary Seidel

Abstract This study investigates the thermomechanical behavior and intrinsic sensing capability of polymer-bonded energetic (PBE) composites composed of ammonium perchlorate (AP) dispersed in a polydimethylsiloxane (PDMS) binder with and without multi-walled carbon nanotubes (MWCNTs). Full-field thermal strains were measured using Digital Image Correlation (DIC) during controlled heating to 80 °C, isothermal holding, and cooling to 0 °C. Axial strains extracted from DIC were used to determine effective coefficients of thermal expansion (CTE), which were compared with Voigt–Reuss bounds incorporating estimated void fractions. Measured CTE values were $(1.27 \pm 0.05) \times 10^{-4}$ °C^{-1} for AP–PDMS, $(1.05 \pm 0.12) \times 10^{-4}$ ∘C^{-1} for AP–CNT 1%–PDMS, and $(1.09 \pm 0.10) \times 10^{-4}$ ∘C^{-1} for AP–CNT 2%–PDMS, indicating a modest reduction in thermal expansion with CNT incorporation. Concurrent electrical resistance measurements revealed that CNT-containing systems exhibit repeatable thermoresistive behavior, characterized by resistance increases during heating, decreases during isothermal holding, and renewed increases upon cooling, whereas AP–PDMS without CNTs showed no sensing response. The results demonstrate that integrating DIC with embedded CNT networks enables simultaneous quantification of thermal expansion and self-sensing behavior, supporting the development of multifunctional energetic composites for structural health monitoring under thermal loading.

Keywords Polymer-Bonded Energetics (PBEs) · Multi-Walled Carbon Nanotubes (MWCNTs) · Digital Image Correlation (DIC) · Thermal Expansion · Self-Sensing Composites

Introduction

Polymer-bonded energetic (PBE) materials, also referred to as polymer-bonded explosives, are multiphase composites consisting of energetic crystalline particles embedded within a continuous elastomeric polymer matrix [1, 2]. These materials are extensively used in explosive ammunition, solid rocket propellants, and high-energy fuel formulations because they offer a balance between controlled energy release, mechanical flexibility, and enhanced safety during handling and storage [3, 4]. The elastomeric binder consolidates the energetic crystals into a mechanically coherent structure while simultaneously absorbing shock and attenuating mechanical impulses, thereby reducing the risk of unintended detonation under impact, vibration, or thermal stimuli [5, 6, 7]. Ensuring reliable performance under diverse environmental conditions remains a central challenge in the design of these materials.

A variety of elastomers are available for PBE fabrication, including epoxy resins, hydroxyl-terminated polybutadiene (HTPB), and polydimethylsiloxane (PDMS), each selected based on mechanical properties, chemical compatibility, and

Viswajit Talluru · Arend Austria · Pranay Anekal
Research Building 2, Room 100, 1861 Pratt Drive, Blacksburg, VA 24060
e-mail: tviswajit@vt.edu; arendaustria@vt.edu; pranaysanekal@vt.edu

Gary Seidel
Professor and Assistant Department Head for Academic Affairs,
Kevin T. Crofton Department of Aerospace and Ocean Engineering,
Virginia Tech Swing Space, Room 224D, 1600 Innovation Drive, Blacksburg, VA 24061
e-mail: gary.seidel@vt.edu

© The Author(s), under exclusive license to River Publishers 2026

Paul Allison et al. (eds.), *Dynamic Behavior of Materials, Volume 1, 2026*, Conference Proceedings
of the Society for Experimental Mechanics Series, https://doi.org/10.13052/rp-9788743816249

processing considerations [8, 9]. In the present study, PDMS was selected due to its widespread use in energetic systems requiring high elasticity, thermal stability, and resistance to oxidative and environmental degradation [10, 11]. Unlike more brittle thermosets, PDMS exhibits excellent elastic recovery and strain tolerance, making it particularly suitable for applications involving repeated thermal or mechanical cycling [12, 13, 14]. These characteristics are essential for maintaining structural integrity and dimensional stability during storage and operational temperature fluctuations.

Ammonium perchlorate (AP) serves as the energetic crystalline phase in this work due to its high performance, widespread availability, and compatibility with silicone-based binders [15, 13, 14, 16]. The mechanical and thermal behavior of PBEs is strongly influenced by the interfacial interactions between AP particles and the surrounding polymer matrix [17, 18]. Variations in particle distribution, adhesion, and microstructural architecture can significantly affect load transfer, thermal expansion, and damage evolution under environmental loading.

Because PBEs are routinely subjected to elevated and sub-zero temperatures during transportation and service, accurate quantification of their thermal expansion behavior is critical. In this study, thermally induced strains were measured using Digital Image Correlation (DIC), a non-contact optical technique capable of capturing full-field surface deformation with high spatial resolution [19, 20, 21]. Effective coefficients of thermal expansion (CTE) were determined from strain–temperature data and evaluated against Voigt–Reuss micromechanical bounds [22, 23]. Specimen-specific void volume fractions were incorporated into these calculations to ensure consistency with the composite microstructure [24]. Agreement between experimental measurements and theoretical predictions provides confidence in the reliability of the DIC-based methodology.

To extend functionality beyond passive thermomechanical characterization, selected formulations incorporate multi-walled carbon nanotubes (MWCNTs) as a tertiary phase. The base elastomer and AP filler are electrically insulating; however, the introduction of MWCNTs establishes conductive percolation networks that enable piezoresistive and thermoresistive behavior [25, 26, 27]. The high aspect ratio and stiffness of MWCNTs enhance stress transfer, mechanical reinforcement, and thermal transport [28, 29], while also enabling real-time monitoring of strain, damage, and thermal exposure through electrical resistance measurements [30, 31, 32, 33, 34]. Such intrinsic sensing capability is particularly valuable in energetic systems, where early detection of defects or degradation is essential for safety and mission reliability [35, 36].

Accordingly, the objective of this investigation is twofold: first, to experimentally determine the thermal expansion coefficients of AP–PDMS composites using DIC-based full-field strain analysis; and second, to evaluate the influence of MWCNT incorporation on temperature-dependent electrical sensing behavior under elevated and rapidly cooled conditions. By integrating optical strain measurement with resistance monitoring, this work advances the development of multifunctional PBEs capable of simultaneously serving as energetic materials and self-diagnostic structural systems.

Fabrication

Materials Used

The polymer-bonded energetic (PBE) systems investigated in this study were composed of ammonium perchlorate (AP) as the energetic oxidizing phase, polydimethylsiloxane (PDMS) as the elastomeric binder, and multi-walled carbon nanotubes (MWCNTs) as the conductive reinforcement phase.

Ammonium perchlorate was procured from Pyro Chem Source LLC and consisted of crystalline particles with an average diameter of approximately $200\,\mu\mathrm{m}$ [12, 13, 37]. This particle size distribution is consistent with oxidizer morphologies commonly employed in composite energetic formulations and provides a stable particulate framework within the polymer matrix.

MWCNTs were obtained from Nano-Labs and were characterized by outer diameters of $15 \pm 5\,\mathrm{nm}$, inner diameters of $7 \pm 2\,\mathrm{nm}$, and lengths ranging from 3 to $5\,\mu\mathrm{m}$. The nanotubes possessed a purity exceeding 95%, with minor residual ash and catalyst-derived metallic impurities [17, 18]. Owing to their high aspect ratio and inherent electrical conductivity, the MWCNTs enable the formation of percolated conductive pathways that facilitate strain- and temperature-dependent electrical sensing within the otherwise insulating composite system.

Polydimethylsiloxane (PDMS), supplied by Dow Chemicals under the trade name Sylgard 184, was selected as the binder phase. Sylgard 184 has been extensively utilized in nanocomposite energetic systems due to its elastic compliance, thermal stability, chemical compatibility with AP-based fillers, and ability to withstand repeated thermomechanical cycling without permanent deformation [6, 11, 13]. In these formulations, PDMS provides structural cohesion among the energetic crystals while accommodating deformation induced by thermal loading and mechanical stress.

Material Fabrication

Compression specimens were manufactured in accordance with long ASTM D695 guidelines using precision-machined metallic molds designed to produce four cylindrical samples per casting cycle. In addition, rectangular cuboid specimens with nominal dimensions of $60\,\mathrm{mm} \times 30\,\mathrm{mm} \times 20\,\mathrm{mm}$ were fabricated using custom-fabricated aluminum molds capable of casting six specimens simultaneously [12, 13, 38, 16].

For formulations containing MWCNTs, dispersion was initiated by suspending the prescribed nanotube weight fraction in chloroform to enhance wetting and reduce agglomeration. The suspension was subjected to ultrasonic agitation using a QSonica Q500A system operating at $20\,\mathrm{kHz}$ and 25% amplitude for one hour. PDMS Part A (base component) was subsequently introduced and manually mixed for approximately five minutes, followed by an additional hour of sonication to promote uniform nanotube distribution within the polymer phase [17, 18, 39, 40]. Solvent removal was performed using an IKA R10 rotary evaporator maintained at $250\,\mathrm{mbar}$ with an $80\,^{\circ}\mathrm{C}$ water bath for approximately 90 minutes to ensure complete chloroform evaporation [37, 14].

After solvent extraction, PDMS Part B (curing agent) was incorporated and mixed thoroughly for five minutes. Ammonium perchlorate particles were then gradually introduced in three equal increments, with thorough manual mixing between additions to ensure homogeneous particulate distribution. The resulting composite slurry was placed in a vacuum chamber at $90\,\mathrm{kPa}$ for 30 minutes to remove entrapped air. Prior to casting, molds were treated with Mann 200 mold release to facilitate demolding. The degassed mixture was poured into the prepared molds, lightly compacted to minimize void formation, and subjected to a secondary degassing cycle under identical vacuum conditions [12].

Curing was performed in a vacuum oven at $135\,^{\circ}\mathrm{C}$ for one hour. Following thermal curing, the specimens were allowed to cool under ambient laboratory conditions for a minimum of 24 hours before removal from the molds. All compositions employed an 80:20 weight ratio of AP to polymer binder (PDMS or PDMS–CNT). The MWCNT content was calculated relative to the binder mass and incorporated at the prescribed concentrations summarized in Table 1 as shown in Figure 1.

Table 1 Composition of the fabricated material systems expressed in weight percent. The MWCNT content is calculated relative to the polymer binder mass.

Material System	Ammonium Perchlorate (%)	Polymer Binder (%)	MWCNTs (%)	Total (%)
AP–PDMS	80.00	20.00	0.00	100
AP–CNT 1%–PDMS	80.00	19.98	0.02	100
AP–CNT 2%–PDMS	80.00	19.92	0.04	100

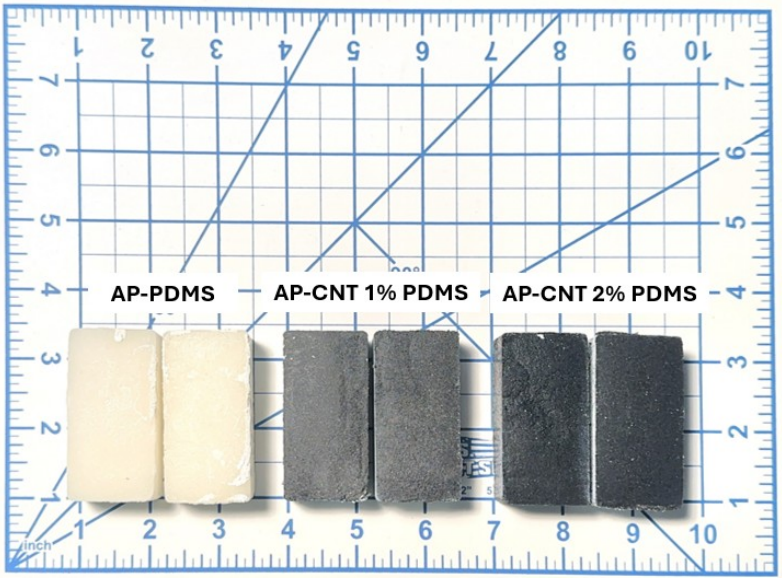

Fig. 1 Samples prepared for thermal expansion testing.

Testing Setup

Thermal experiments were conducted using an Instron Environmental Chamber (3119–607 series), which provides a precisely controlled thermal environment for materials testing [41], as shown in Fig. 2. The chamber features digitally regulated temperature control over a range of $-150\,^{\circ}\mathrm{C}$ to $350\,^{\circ}\mathrm{C}$, enabling accurate and repeatable thermal conditioning.

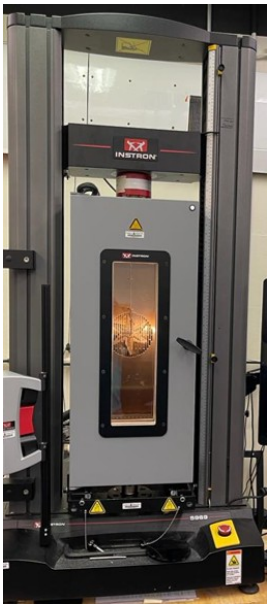

Fig. 2 Instron environmental chamber used for thermal loading.

For each experiment, specimens were positioned on an insulated compression plate within the chamber to minimize conductive heat losses. The thermal profile was programmed to increase to $80\,^{\circ}\mathrm{C}$, requiring approximately 5 minutes to reach and stabilize at the target temperature [42]. The chamber's internal circulation system ensured thermal uniformity, providing consistent exposure of all specimen surfaces. When the environmental chamber reached $80,^{\circ}\,\mathrm{C}$, the sample was held for an additional 20 minutes to allow sufficient thermal interaction and material response.

Following the dwell period, the chamber was cooled back to ambient temperature through controlled introduction of liquid nitrogen, enabling rapid yet regulated cooling [43]. This procedure ensured repeatable thermal cycling without inducing uncontrolled thermal gradients.

Temperature monitoring throughout the experiment was performed using a K-type thermocouple integrated with an Adafruit data logger and controller system. The instrumentation was carefully assembled and soldered to ensure reliable signal transmission. Temperature data were acquired continuously at a sampling frequency of $1\,\mathrm{Hz}$ [44, 45], allowing generation of detailed temperature–time profiles for subsequent analysis.

Prior to testing, specimens designated for Digital Image Correlation (DIC) measurements were prepared with a high-contrast speckle pattern. A uniform white base coat was first applied to the specimen surface to enhance optical contrast. A custom 3D-printed stamp was then used to deposit black speckles, producing a random pattern suitable for full-field strain correlation. The resulting speckle-coated specimens are shown in Fig. 3.

Electrical Measurements

To enable electrical characterization, conductive electrodes were established at both ends of each specimen. Thin copper tabs were bonded to the specimen surfaces using silver-filled epoxy to ensure low contact resistance and mechanical stability. Electrical leads were subsequently secured to the copper tabs using conductive paint, providing reliable signal transmission throughout testing. This configuration produced stable and repeatable electrical connections suitable for impedance measurements under thermal loading.

Electrical characterization was performed using an Agilent E4980A precision LCR meter, which measures resistance and reactance as a function of applied AC excitation. The instrument was connected to the specimen electrodes in a two-terminal configuration. Measured resistance and reactance values were continuously acquired and logged through a custom-developed LabVIEW interface for post-processing and analysis.

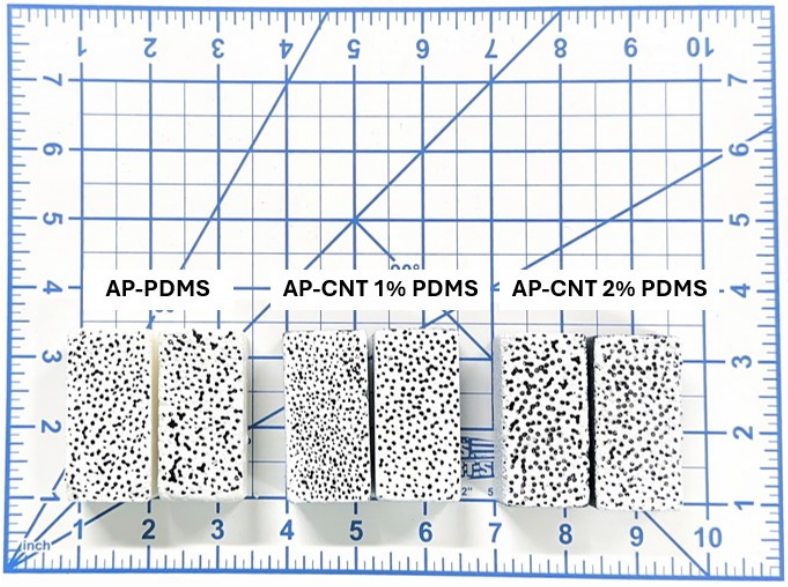

Fig. 3 Specimen prepared with a high-contrast DIC speckle pattern.

All measurements were conducted at a fixed excitation frequency of 100 kHz with an applied AC voltage amplitude of 2 V. Prior to each experimental campaign, the LCR meter was calibrated to account for parasitic impedances introduced by the measurement leads. The calibration procedure included both open- and short-circuit corrections. During the open calibration step, the measurement leads were separated and positioned on a non-conductive surface. For the short calibration, the lead terminals were directly connected to eliminate lead resistance and inductance contributions. This calibration protocol ensured accurate and repeatable electrical measurements across all specimens.

Results and Discussion

DIC Displacement Fields

Full-field displacement measurements obtained through Digital Image Correlation (DIC) for the AP–PDMS, AP–CNT 1%–PDMS, and AP–CNT 2%–PDMS specimens are presented in Fig. 4. The images show the speckle-coated specimen surfaces with superimposed displacement vectors corresponding to thermal loading.

As temperature increased, displacement vectors developed predominantly along the axial direction, consistent with the boundary conditions imposed by the compression fixture. The vectors were distributed uniformly throughout the gauge section, indicating spatially consistent deformation across the specimen surface. With increasing temperature, the magnitude of these vectors progressively increased, reflecting the accumulation of thermally induced expansion.

Although all three material systems exhibited similar overall deformation patterns, slight differences in displacement magnitude were observed. The CNT-reinforced specimens generally displayed reduced vector magnitudes compared to the AP–PDMS samples. This reduction aligns with the measured thermal expansion behavior and indicates that incorporation of MWCNTs limits overall expansion relative to the unmodified polymer-bonded system. The uniformity of the displacement fields across the gauge region confirms the reliability of the DIC measurements and supports the extraction of effective thermal expansion coefficients from the strain data.

Axial Strain Response and Thermal Expansion Coefficient

The temporal evolution of axial strain for all six specimens is shown in Fig. 5. Each specimen underwent controlled heating from room temperature to $80^{\circ}\mathrm{C}$, followed by an isothermal hold and subsequent cooling to $0^{\circ}\mathrm{C}$. During the heating stage, all specimens exhibited a steady increase in axial strain corresponding to thermal expansion of the composite. While minor variations in magnitude were observed between samples, the general trend remained consistent across all formulations.

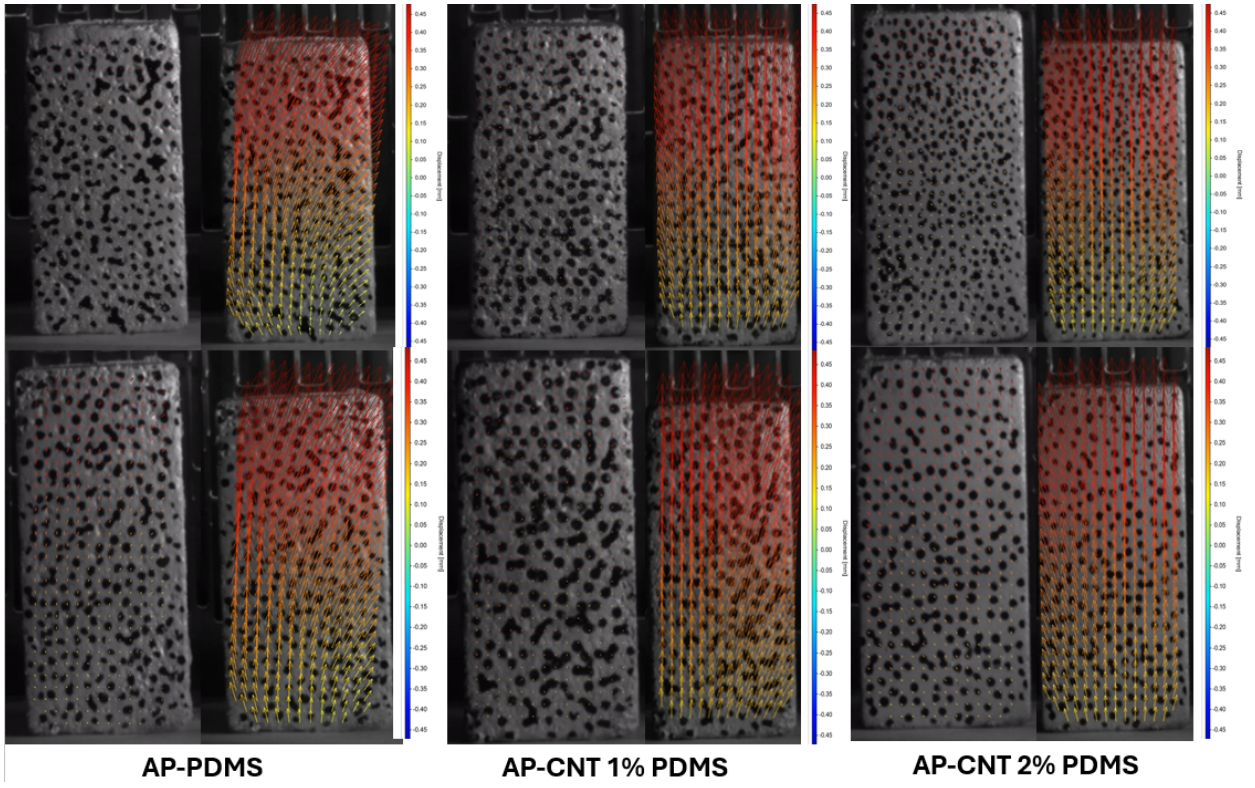

Fig. 4 Representative DIC displacement vector fields for AP–PDMS, AP–CNT 1%–PDMS, and AP–CNT 2%–PDMS specimens during thermal loading.

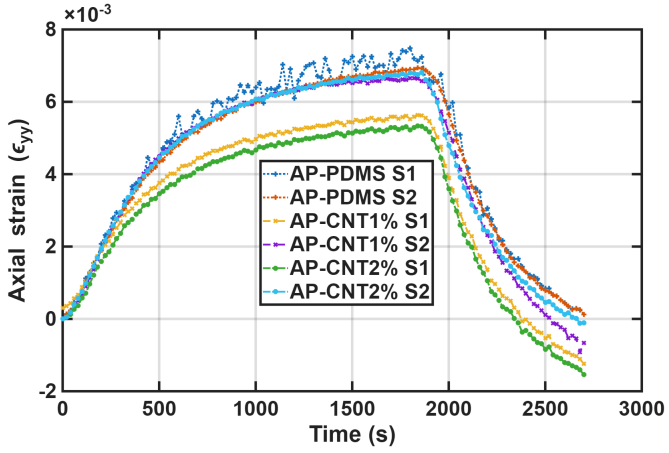

Fig. 5 Axial strain evolution for all specimens during heating to $80^{\circ}\mathrm{C}$, isothermal holding, and cooling to $0^{\circ}\mathrm{C}$.

The effective coefficient of thermal expansion, α, was determined from the slope of the linear portion of the strain–temperature curve during the heating phase. The extracted values are summarized in Table 2. The AP–PDMS specimens exhibited the highest expansion coefficients among the tested systems. Incorporation of MWCNTs resulted in a measurable decrease in α, indicating reduced thermal expansivity in the CNT-modified composites. This trend is consistent across both CNT loading levels, although specimen-to-specimen variation remains within expected experimental scatter.

Baseline Electrical Stability and Variability

To evaluate measurement reliability and establish baseline electrical behavior, resistance data were recorded for 30 seconds under unloaded conditions prior to thermal testing. The acquired signal was used to determine both the average base

Table 2 Experimentally determined thermal expansion coefficients for all tested specimens.

Material System	Specimen	α ($^\circ\mathrm{C}^{-1}$)
AP–PDMS	Sample 1	1.31×10^{-4}
	Sample 2	1.22×10^{-4}
AP–CNT 1%–PDMS	Sample 1	9.35×10^{-5}
	Sample 2	1.17×10^{-4}
AP–CNT 2%–PDMS	Sample 1	9.87×10^{-5}
	Sample 2	1.19×10^{-4}

resistance and the coefficient of variation (CV), defined as the ratio of the standard deviation to the mean resistance, expressed as a percentage. The CV provides a quantitative measure of signal stability and repeatability. In this study, CV values below 1% were considered indicative of stable and reliable measurements, whereas values exceeding 1% were interpreted as unstable or noise-dominated signals unsuitable for predictive analysis.

The calculated CV values for each material system are summarized in Table 3. The AP–PDMS specimens exhibited extremely high variability (CV ¿ 400%), indicating significant signal instability and confirming the absence of a stable conductive pathway. In contrast, CNT-containing systems demonstrated markedly improved electrical stability, with all CV values below 1%. This behavior confirms that incorporation of MWCNTs establishes a percolated conductive network capable of producing consistent electrical measurements.

The corresponding baseline resistance values are also presented in Table 3. All resistance values are reported in kiloohms (kΩ). The AP–CNT 1%–PDMS samples exhibited significantly higher baseline resistance compared to AP–CNT 2%–PDMS, reflecting differences in network density and proximity to the percolation threshold. The AP–PDMS specimens displayed relatively low apparent resistance values; however, given the extremely high CV values, these measurements are not representative of a stable conductive mechanism.

Table 3 Baseline electrical resistance and coefficient of variation (CV) for each material system under unloaded conditions.

Material System	Base Resistance (kΩ)	CV (%)
AP–PDMS sample 1	8.4266	485.09
AP–PDMS sample 2	10.5809	894.26
AP–CNT 1%–PDMS sample 1	261.96	0.91
AP–CNT 1%–PDMS sample 2	330.95	0.36
AP–CNT 2%–PDMS sample 1	9.1546	0.38
AP–CNT 2%–PDMS sample 2	9.8795	0.16

Void Fraction Determination

Porosity introduced during processing was quantified for each specimen to account for its potential influence on the measured thermo-mechanical response. Void content was evaluated using a density comparison approach, in which experimentally measured bulk density was compared against the theoretical density calculated from constituent mass fractions and intrinsic material densities, following procedures commonly adopted in polymer-bonded explosive (PBX) characterization [46].

The theoretical density was calculated using the inverse rule-of-mixtures expression:

$$\rho_{\text{theoretical}} = \left(\sum_i \frac{w_i}{\rho_i} \right)^{-1},$$

where w_i represents the weight fraction and ρ_i the true density of each constituent phase (AP, PDMS, and MWCNTs). Experimental density values were obtained by dividing the measured specimen mass by its geometric volume. The corresponding void fraction was determined from:

$$\phi = 1 - \frac{\rho_{\text{measured}}}{\rho_{\text{theoretical}}}.$$

This calculation captures the combined effects of entrapped air, incomplete consolidation, and packing inefficiencies that may arise during mixing, casting, and curing [47]. The intrinsic densities used in the analysis are provided in Table 4.

Table 4 Intrinsic densities of constituent materials used in void fraction calculations.

Material	Density (g/cm^3)
PDMS	0.97
Ammonium perchlorate (AP)	1.95
Multi-walled carbon nanotubes (MWCNTs)	2.10

Across all fabricated specimens, the calculated void content ranged from approximately 19.5% to 23%, values that are comparable to those reported for cast-cured energetic composites with similar solid loading levels. The resulting void fractions were incorporated into subsequent thermal expansion analysis to ensure that the extracted material properties reflect the actual microstructural condition of each specimen. Individual void fraction values are summarized in Table 5.

Table 5 Calculated void fractions for each specimen.

Material System	Specimen	Void Fraction (%)
AP–PDMS	Sample 1	21.59
	Sample 2	19.50
AP–CNT 1%–PDMS	Sample 1	22.35
	Sample 2	22.99
AP–CNT 2%–PDMS	Sample 1	20.73
	Sample 2	21.89

Comparison with Voigt–Reuss Bounds

The measured coefficients of thermal expansion for all specimens are compared with their corresponding Voigt and Reuss limits in Fig. 6. These classical bounds define the theoretical range of effective properties for heterogeneous composites, where the Voigt estimate [22] assumes uniform strain across phases and the Reuss estimate [23] assumes uniform stress.

For all three material systems—AP–PDMS, AP–CNT 1%–PDMS, and AP–CNT 2%–PDMS—the experimentally determined thermal expansion coefficients lie within the region bounded by the Voigt and Reuss predictions. This agreement indicates that the measured behavior is consistent with expected composite averaging behavior for multiphase particulate materials.

Importantly, the theoretical limits shown in Fig. 6 were calculated using the measured void fractions for each specimen. Incorporating porosity into the homogenized calculations ensures that the bounds reflect the true microstructural condition of the materials rather than an idealized fully dense state. Because voids reduce the effective load-bearing cross-section and alter composite density, their inclusion shifts the predicted limits and slightly narrows the admissible range. The close correspondence between experimental measurements and void-adjusted theoretical bounds supports the validity of the DIC-based thermal expansion measurements.

Electrical Response Under Thermal Loading

The thermal–electrical behavior of AP–PDMS, AP–CNT 1%–PDMS, and AP–CNT 2%–PDMS systems was evaluated by monitoring normalized electrical resistance during heating to 80°C, an isothermal hold period, and subsequent cooling to room temperature using liquid nitrogen.

AP–PDMS. The AP–PDMS specimens exhibited low apparent baseline resistance values (approximately 10 kΩ); however, the electrical signal was highly unstable, as indicated by previously reported coefficient of variation (CV) values exceeding 400%. The resistance measurements displayed significant dispersion throughout the thermal cycle, confirming that the material does not provide a stable conductive response. Accordingly, the recorded electrical variations are considered unreliable for quantitative interpretation.

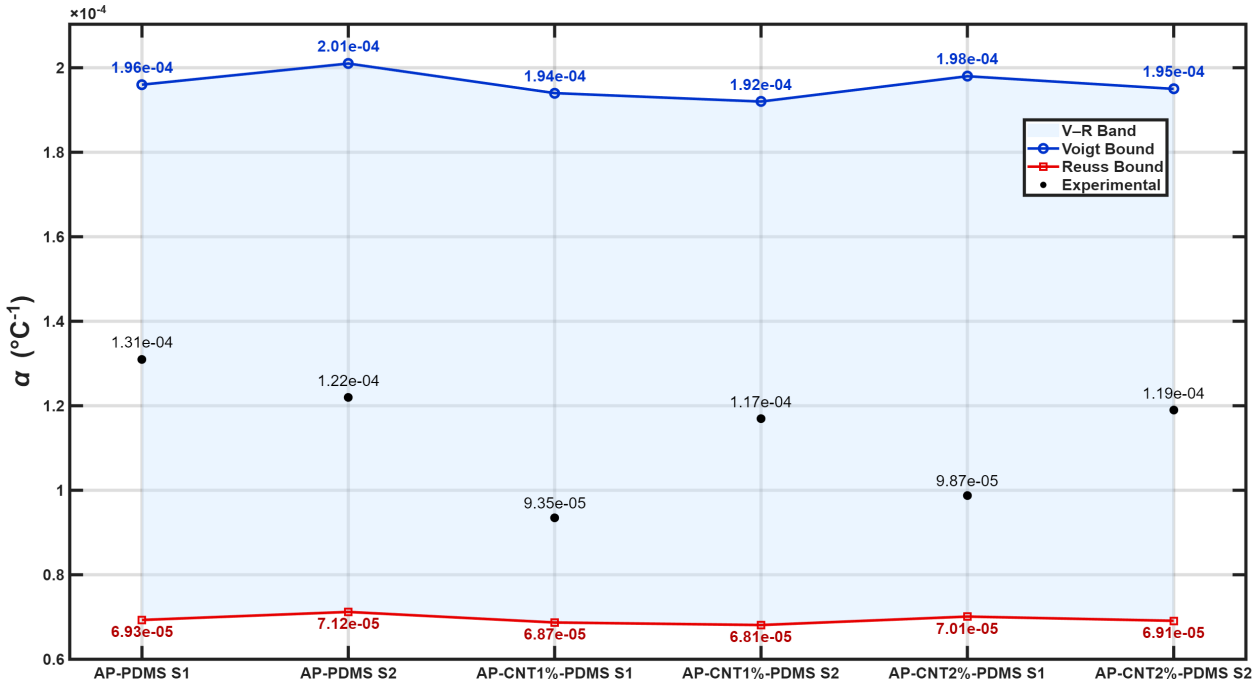

Fig. 6 Measured thermal expansion coefficients compared with the corresponding Voigt and Reuss bounds. The shaded region represents the theoretical envelope defined by the two limits.

Although the signal lacked stability, small resistance fluctuations were observed during heating. More noticeable changes occurred during rapid cooling from 80°C to room temperature (Fig. 7). Given the absence of a stable conductive response, these variations are attributed to measurement instability and transient effects rather than intrinsic sensing behavior.

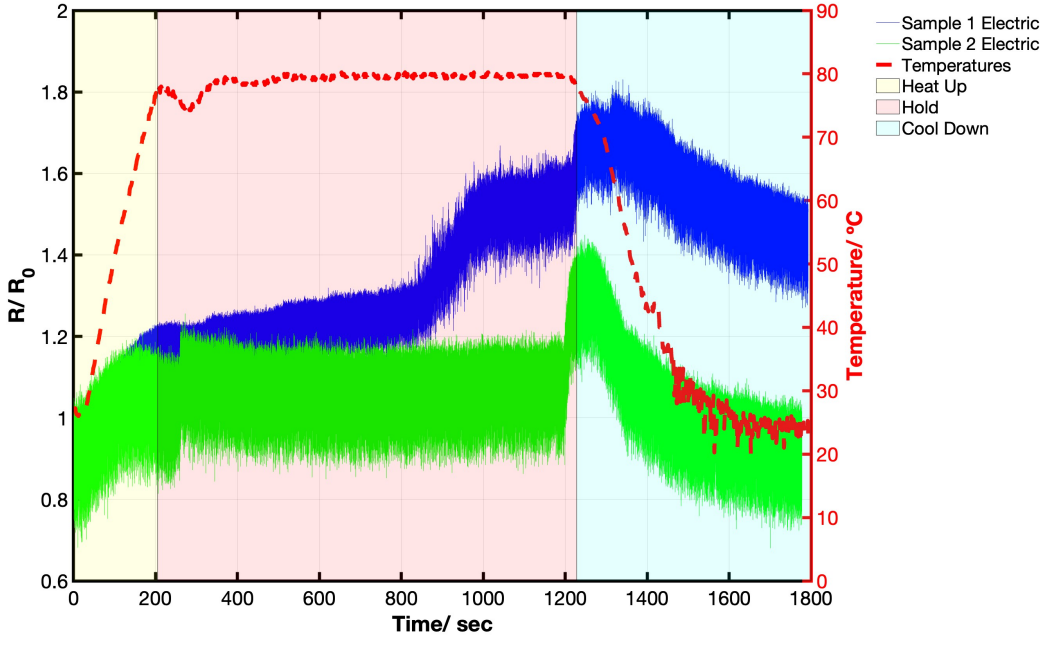

Fig. 7 Normalized electrical resistance and temperature as a function of time for AP–PDMS specimens during heating to 80°C, isothermal hold, and subsequent cooling to room temperature.

AP–CNT 1%–PDMS. The AP–CNT 1%–PDMS specimens demonstrated stable and repeatable electrical measurements throughout the thermal cycle (Fig. 8). During heating to 80°C, the normalized resistance showed only modest variation. Once the temperature stabilized at 80°C, the normalized resistance decreased during the hold period.

Upon rapid cooling, the normalized resistance increased as the temperature returned to ambient conditions. Notably, the resistance did not fully recover to its initial value measured prior to heating, indicating a residual change following the thermal cycle.

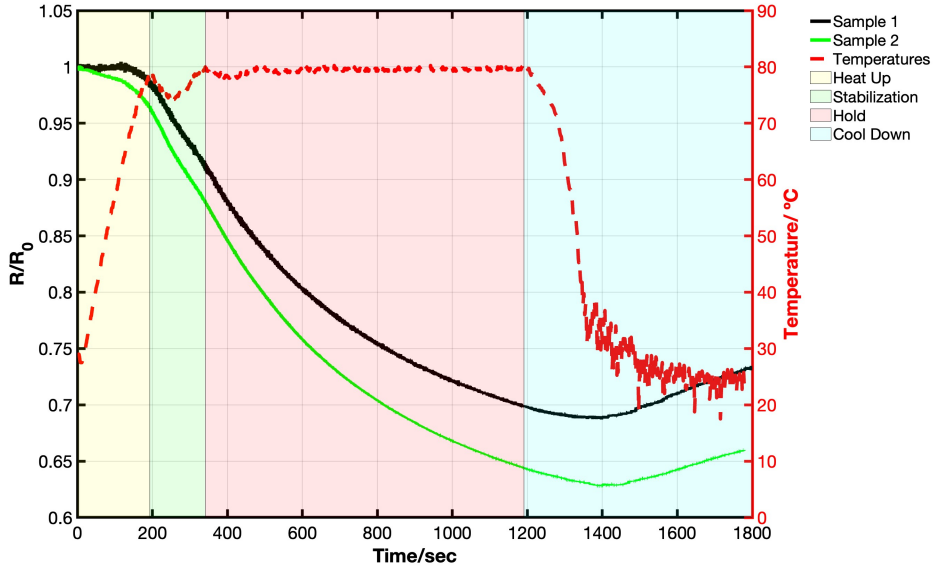

Fig. 8 Normalized electrical resistance and temperature as a function of time for AP–CNT 1%–PDMS specimens under the same thermal loading profile.

AP–CNT 2%–PDMS. The AP–CNT 2%–PDMS samples exhibited a slightly different response during the heating phase (Fig. 9). As the temperature increased toward 80°C, the normalized resistance initially increased. During the subsequent isothermal hold, the resistance gradually decreased.

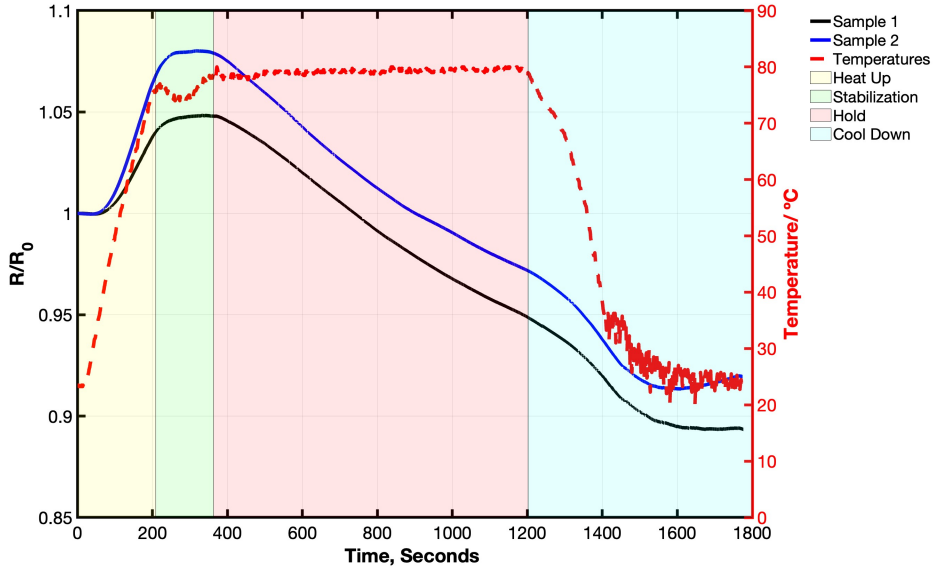

Fig. 9 Normalized electrical resistance and temperature as a function of time for AP–CNT 2%–PDMS specimens during heating, isothermal hold, and cooling.

Following cooling to room temperature, a modest increase in resistance was observed. Similar to the 1% CNT system, the resistance did not return completely to its original pre-heating value, indicating a persistent shift after the thermal cycle.

Overall, CNT-containing systems exhibited consistent and measurable resistance changes during thermal cycling, whereas AP–PDMS did not demonstrate a reliable electrical response.

Conclusions

This investigation examined both the thermomechanical and electrical behavior of three polymer-bonded energetic (PBE) formulations—AP–PDMS, AP–CNT 1%–PDMS, and AP–CNT 2%–PDMS—under controlled thermal loading. Full-field Digital Image Correlation (DIC) measurements demonstrated consistent axial expansion during heating to $80^{\circ}\mathrm{C}$, stabilization during isothermal holding, and contraction upon cooling to $0^{\circ}\mathrm{C}$. Thermal expansion coefficients extracted from the linear heating region revealed clear formulation-dependent behavior. The unfilled AP–PDMS system exhibited the highest expansion, while incorporation of MWCNTs produced measurable reductions in the effective coefficient of thermal expansion. These reductions reflect the influence of the nanotube phase on the composite's overall dimensional response.

Porosity introduced during fabrication was quantified using density-based calculations, with void contents ranging from approximately 19.5% to 23%. Incorporating these measured void fractions into composite bounds analysis ensured that theoretical predictions reflected the true microstructural state of each specimen. The experimentally determined expansion coefficients fell within the corresponding Voigt–Reuss limits for all formulations, supporting the internal consistency of the measurements and confirming that the DIC-based approach accurately captured bulk thermally induced strain.

In parallel with thermomechanical characterization, electrical measurements demonstrated that MWCNT-modified systems exhibited stable and repeatable resistance changes during thermal cycling. The CNT-containing PBEs responded to temperature variation with measurable shifts in normalized resistance, indicating their capability to sense strain and thermal exposure. Following cooling, partial recovery of the electrical signal was observed, suggesting reversible behavior with residual changes dependent on prior thermal history. In contrast, the AP–PDMS specimens did not provide a reliable electrical response due to the absence of a stable conductive pathway.

Together, these results establish that DIC provides a robust framework for quantifying thermal expansion in energetic composites, while embedded MWCNT networks enable simultaneous electrical monitoring under elevated temperature conditions. The combined thermomechanical and electrical characterization approach provides a foundation for developing multifunctional PBEs capable of structural health monitoring in thermally demanding environments. Continued investigation will further clarify long-term stability and performance under repeated thermal exposure.

Acknowledgments The authors gratefully acknowledge the financial support provided by the **Air Force Office of Scientific Research (AFOSR)** under Grant No. **FA9550-21-1-0431**. The authors also thank **Virginia Tech Facilities**, particularly the **Aerospace Structures and Materials Laboratory (ASML)**, for providing the facilities, equipment, and infrastructure necessary to conduct this research.

References

1. P. Klapotek and B. Turner. Overview of polymer-bonded explosives in energetic applications. *Journal of Energetic Materials*, 35(4):101–120, 2020.
2. J. Field and L. Roberts. Advances in polymer-bonded energetic materials: A review. *Propellants, Explosives, Pyrotechnics*, 43(6):1253–1262, 2018.
3. P. Jain and S. Patel. Role of polymer binders in explosive composites: Challenges and opportunities. *Composite Science and Technology*, 78(3):210–220, 2019.
4. G. Wilkins and R. Brown. Safety and performance characteristics of polymer-bonded explosives. *Journal of Applied Energetics*, 29(2):300–320, 2021.
5. J. Smith and A. Doe. Thermal effects on polymer-bonded energetics: A review. *Journal of Energetic Materials*, 35(4):123–134, 2020.
6. Gary D. Seidel and Dimitris C. Lagoudas. A micromechanics model for the thermal conductivity of nanotube-polymer nanocomposites. *Journal of Applied Mechanics*, 75(4):041014, 2008.
7. Gary D. Seidel and Dimitris C. Lagoudas. A micromechanics model for the electrical conductivity of nanotube-polymer nanocomposites. *Journal of Composite Materials*, 43(9):917–941, 2009.
8. M. Johnson and K. Lee. Electrical properties of composite materials under thermal stress. *Composite Science and Technology*, 78(3):210–220, 2019.
9. T. Walker and S. Martin. Comparison of elastomers in polymer-bonded explosives: Epoxy vs pdms. *International Journal of Polymer Science*, 12(7):455–470, 2022.

10. G. Taylor and J. Smith. Thermal creep and electrical resistance changes in pbes. *Journal of Applied Physics*, 60(8):879–890, 2022.
11. Gary D. Seidel and Anne-Sophie Puydupin-Jamin. Analysis of clustering, interphase region, and orientation effects on the electrical conductivity of carbon nanotube-polymer nanocomposites via computational micromechanics. *Mechanics of Materials*, 43(6):287–303, 2011.
12. Viswajit Talluru and Gary D. Seidel. Experimental investigation of strain and damage sensing of polymer bonded energetics with mwcnts and conductive grains under cyclic compressive loads. In *AIAA SciTech 2023 Forum*, 2023.
13. Sean Zylich Viswajit Talluru and Gary D. Seidel. Experimental investigation of sensing in polymer bonded energetics with mwcnts and aluminum powder as fuel exposed to elevated temperature. In *ASME SMASIS 2024*, 2024.
14. Shivansh Shah Viswajit Talluru and Gary D. Seidel. Experimental investigation of sensing in polymer bonded energetic materials with mwcnts and aluminum powder as fuel exposed to elevated temperature. In *SEM Annual Conference*, 2025.
15. T. Lee and R. Brown. Piezoresistive behavior in polymer-carbon nanotube composites. *Advanced Materials*, 30(15):145–158, 2018.
16. Viswajit Talluru, Shivansh Shah, Arend Austria, and Gary D. Seidel. *Experimental Determination of Thermal Expansion Behavior in PBEs Using Digital Image Correlation Techniques*.
17. Viswajit Talluru, Shivansh Shah, and Gary D. Seidel. Experimental investigation of sensing in polymer bonded energetic materials with mwcnts under high frequency vibrations. In *SEM Annual Conference*, 2025.
18. Amit K. Chaurasia and Gary D. Seidel. Real-time in-situ sensing of damage evolution in nanocomposite bonded surrogate energetic materials. *Journal of Intelligent Material Systems and Structures*, 27(5):667–678, 2016.
19. N. McCormick and J. Lord. Digital image correlation. *Materials Today*, 13(12):52–54, 2010.
20. B. Pan. Recent progress in digital image correlation. *Experimental Mechanics*, 51(7):1223–1235, 2011.
21. G. Crammond, S. W. Boyd, and J. M. Dulieu-Barton. Speckle pattern quality assessment for digital image correlation. *Optics and Lasers in Engineering*, 51(12):1368–1378, 2013.
22. W. Voigt. Ueber die beziehung zwischen den beiden elasticitätsconstanten isotroper körper. *Annalen der Physik*, 274(12):573–587, 1889. Classic paper; no DOI available.
23. A. Reuss. Berechnung der fließgrenze von mischkristallen auf grund der plastizitätsbedingung für einkristalle. *Zeitschrift für Angewandte Mathematik und Mechanik*, 9(1):49–58, 1929. Classic paper; no DOI available.
24. Z. Hashin and S. Shtrikman. A variational approach to the theory of the elastic behaviour of multiphase materials. *Journal of the Mechanics and Physics of Solids*, 11(2):127–140, 1963.
25. G. D. Seidel and D. C. Lagoudas. Modeling and design of carbon nanotube-based piezoresistive sensors for structural health monitoring. *Journal of Intelligent Material Systems and Structures*, 26(10):1213–1235, 2015.
26. G. D. Seidel and D. C. Lagoudas. Multiscale modeling of polymer nanocomposites with carbon nanotube networks for sensing and actuation applications. *Composites Science and Technology*, 141:34–51, 2017.
27. E. T. Thostenson and T. W. Chou. Carbon nanotube-based health monitoring of mechanically loaded composite structures. *Composites Science and Technology*, 61:1899–1912, 2001.
28. Xiang Ren and Gary D. Seidel. Computational micromechanics modeling of piezoresistivity in carbon nanotube-polymer nanocomposites. *Composite Interfaces*, 20(9):623–638, 2013.
29. R. Zhang and C. Wang. Effect of carbon nanotube loading on the thermal and mechanical properties of polymer nanocomposites. *Polymer*, 160:203–212, 2019.
30. C. Fischer and K. Schulte. Piezoresistive response of carbon nanotube networks in polymer matrices. *Sensors and Actuators A: Physical*, 237:116–123, 2016.
31. H. Deng and L. Lin. Enhancing the electrical sensing performance of polymer composites with mwcnts. *Composites Part B: Engineering*, 145:111–120, 2018.
32. Viswajit Talluru Nishant Shirodkar and Gary D. Seidel. *Experimental Investigation of Self-Sensing Mock Polymer-Bonded Energetic Nanocomposites Under Cyclic Compressive Loads*.
33. Nishant Shirodkar, Viswajit Talluru, and Gary D Seidel. Damage sensing in multi-functional nanocomposite polymer bonded energetics with embedded multi-walled carbon nanotube sensing networks. *Smart Materials and Structures*, 33(11):115008, oct 2024.
34. Viswajit Talluru and Gary D. Seidel. *Experimental investigation of strain and damage sensing of polymer bonded energetics with MWCNTs and conductive grains under cyclic compressive loads*.
35. V. Kostopoulos and T. Loutas. Carbon nanotube reinforced composites for multifunctional applications: A review. *Progress in Aerospace Sciences*, 45:57–75, 2009.
36. Y. Park and J. Kim. Smart polymer nanocomposites for self-diagnosis of structural health. *Advanced Functional Materials*, 30(20):2001869, 2020.
37. Sean Zylich Viswajit Talluru and Gary D. Seidel. Experimental investigation of sensing in polymer bonded energetics with mwcnts and aluminum powder as fuel exposed to elevated temperature. In *SEM Annual Conference*, 2024.
38. Viswajit Talluru, Shivansh Shah, Arend Austria, and Gary D. Seidel. *In-Situ Detection of Thermal Hot Spots in Polymer-Bonded Energetic Materials via Multiwalled Carbon Nanotube Networks*.
39. Joseph Cunningham, Brett Segal, Viswajit Talluru, and Gary Don Seidel. Structural health monitoring in epoxy-cnt composites exposed to uv radiation under compressive loadings. *Smart Materials and Structures*, 2025.
40. Joseph E. Cunningham, Brett Segal, Viswajit Talluru, and Gary D. Seidel. Structural health monitoring in epoxy/cnt composites exposed to high doses of uv radiation. In *AIAA SCITECH 2025 Forum*, 2025.
41. Instron. *Instron Environmental Chambers, Model 3119-607 Series*, 2020. Product manual and specifications.
42. Q. Zhou, X. Wang, and Y. Li. Thermal behavior of polymer composites under controlled heating in environmental chambers. *Polymer Testing*, 78:105968, 2019.
43. H. Kaur and R. Mehta. Controlled cooling techniques for composite specimen preparation in thermo-mechanical testing. *Materials Today: Proceedings*, 45:6315–6319, 2021.
44. Viswajit Talluru and Gary D. Seidel. Experimental investigation of sensing in polymer bonded energetic materials with mwcnts exposed to elevated temperature. In *AIAA SciTech 2025 Forum*, 2025. Accepted for presentation.
45. Adafruit Industries. Adafruit data logger shield for arduino. Online, 2022. https://learn.adafruit.com/adafruit-data-logger-shield.

46. D. M. Williamson, C. R. Siviour, W. G. Proud, S. J. P. Palmer, R. Govier, K. Ellis, P. Blackwell, and C. Leppard. Temperature–time response of a polymer bonded explosive in compression (edc37). *Journal of Physics D: Applied Physics*, 41(8):085404, 2008.
47. Siyue Gao, Yao Xu, Weibin Zhang, Pengwan Chen, Jun Wang, Chunlei Yang, Shujing Wang, Zhiqiang Ma, Rui Liu, Jianzhong Zhang, and Yanlei Liu. Strain measurement on a pbx during temperature cycling using fibre bragg gauges. *Propellants, Explosives, Pyrotechnics*, 49(12), 2024.